

Strong interlayer coupling in van der Waals heterostructures built from single-layer chalcogenides

Hui Fang^{a,b}, Corsin Battaglia^{a,b}, Carlo Carraro^c, Slavomir Nemsak^{b,d}, Burak Ozdol^{e,f}, Jeong Seuk Kang^{a,b}, Hans A. Bechtel^g, Sujay B. Desai^{a,b}, Florian Kronast^h, Ahmet A. Unal^h, Giuseppina Conti^{b,d}, Catherine Conlon^{b,d}, Gunnar K. Palsson^{b,d}, Michael C. Martin^g, Andrew M. Minor^{e,f}, Charles S. Fadley^{b,d}, Eli Yablonovitch^{a,b,1}, Roya Maboudian^c, and Ali Javey^{a,b,1}

Departments of ^aElectrical Engineering and Computer Sciences, ^cChemical and Biomolecular Engineering, and ^eMaterials Science and Engineering, University of California, Berkeley, CA 94720; ^bMaterials Sciences Division, ^fNational Center for Electron Microscopy, and ^gAdvanced Light Source, Lawrence Berkeley National Laboratory, Berkeley, CA 94720; ^dDepartment of Physics, University of California, Davis, CA 95616; and ^hHelmholtz-Zentrum Berlin für Materialien und Energie GmbH, D-12489 Berlin, Germany

Contributed by Eli Yablonovitch, March 24, 2014 (sent for review March 10, 2014)

Semiconductor heterostructures are the fundamental platform for many important device applications such as lasers, light-emitting diodes, solar cells, and high-electron-mobility transistors. Analogous to traditional heterostructures, layered transition metal dichalcogenide heterostructures can be designed and built by assembling individual single layers into functional multilayer structures, but in principle with atomically sharp interfaces, no interdiffusion of atoms, digitally controlled layered components, and no lattice parameter constraints. Nonetheless, the optoelectronic behavior of this new type of van der Waals (vdW) semiconductor heterostructure is unknown at the single-layer limit. Specifically, it is experimentally unknown whether the optical transitions will be spatially direct or indirect in such hetero-bilayers. Here, we investigate artificial semiconductor heterostructures built from single-layer WSe₂ and MoS₂. We observe a large Stokes-like shift of ~100 meV between the photoluminescence peak and the lowest absorption peak that is consistent with a type II band alignment having spatially direct absorption but spatially indirect emission. Notably, the photoluminescence intensity of this spatially indirect transition is strong, suggesting strong interlayer coupling of charge carriers. This coupling at the hetero-interface can be readily tuned by inserting dielectric layers into the vdW gap, consisting of hexagonal BN. Consequently, the generic nature of this interlayer coupling provides a new degree of freedom in band engineering and is expected to yield a new family of semiconductor heterostructures having tunable optoelectronic properties with customized composite layers.

MoS₂-WSe₂ heterostructure | Moiré pattern | charge transfer | exciton relaxation | rectifying

Two-dimensional layered transition metal dichalcogenide (TMDC) semiconductors such as MoS₂ and WSe₂ have established themselves as strong contenders for next-generation electronics and optoelectronics (1–6) and are promising building blocks for novel semiconductor heterostructures (7–11). Conventional heterostructures are mainly based on group IV, III-V, or II-VI semiconductors with covalent bonding between atoms at the hetero-interface. Owing to atomic interdiffusion during growth, the resulting atomic-scale interface roughness and composition variation at the hetero-interface inevitably smear the density of states profile and consequently compromise the performance of these heterostructures, especially as the film thicknesses are reduced toward a single atomic layer. In addition, the choice of material components for conventional heterostructures is strongly dictated by lattice mismatch.

In TMDCs, however, individual layers are held together by van der Waals (vdW) forces, without surface dangling bonds (12). Semiconductor heterostructures built up from monolayer TMDCs would in principle offer atomically regulated interfaces and thereby sharp band edges. Theoretical studies have predicted different

electronic structures and optical properties from TMDC hetero-bilayers (13–17); however, to date there have been no experimental results. Whereas previous experimental efforts have focused on graphene-based layered heterostructures (8–11, 18–26), we present an experimental study on the electronic interlayer interaction in a heterostructure built from two single-layer TMDC semiconductors, namely, MoS₂ and WSe₂. The hetero-bilayers are characterized by transmission electron microscopy, X-ray photoelectron microscopy, electron transport studies, and optical spectroscopy to elucidate the band alignments, optoelectronic properties, and the degree of the electronic layer coupling in this novel material system.

The fabrication of WSe₂/MoS₂ hetero-bilayers was realized by stacking individual monolayers on top of each other (see *SI Methods* for details). Fig. 1*A* shows an illustration of the hetero-bilayer, and Fig. 1*B* displays the corresponding optical microscope image of a WSe₂/MoS₂ hetero-bilayer on a Si substrate with 260-nm thermally grown SiO₂. Owing to the 3.8% lattice mismatch, estimated from the bulk lattice constants (12), as well as the unregulated, but in principle controllable, angular alignment (ϕ) between the constituent layers, the heterostructure lattice forms a moiré pattern, clearly visible in the high-resolution transmission electron microscopy (HRTEM) image in Fig. 1*C*. The HRTEM image displays the boundary region between

Significance

A new class of heterostructures consisting of layered transition metal dichalcogenide components can be designed and built by van der Waals (vdW) stacking of individual monolayers into functional multilayer structures. Nonetheless, the optoelectronic properties of this new type of vdW heterostructure are unknown. Here, we investigate artificial semiconductor heterostructures built from single-layer WSe₂ and MoS₂. We observe spatially direct absorption but spatially indirect emission in this heterostructure, with strong interlayer coupling of charge carriers. The coupling at the hetero-interface can be readily tuned by inserting hexagonal BN dielectric layers into the vdW gap. The generic nature of this interlayer coupling is expected to yield a new family of semiconductor heterostructures having tunable optoelectronic properties through customized composite layers.

Author contributions: H.F., C. Carraro, R.M., and A.J. designed research; H.F., C. Carraro, S.N., B.O., J.S.K., H.A.B., S.B.D., F.K., A.A.U., G.C., C. Conlon, G.K.P., and M.C.M. performed research; H.F., C.B., C. Carraro, S.N., B.O., G.C., A.M.M., C.S.F., E.Y., R.M., and A.J. analyzed data; and H.F., C.B., and A.J. wrote the paper.

The authors declare no conflict of interest.

Freely available online through the PNAS open access option.

¹To whom correspondence may be addressed. E-mail: eliy@eecs.berkeley.edu or ajavey@eecs.berkeley.edu.

This article contains supporting information online at www.pnas.org/lookup/suppl/doi:10.1073/pnas.1405435111/-DCSupplemental.

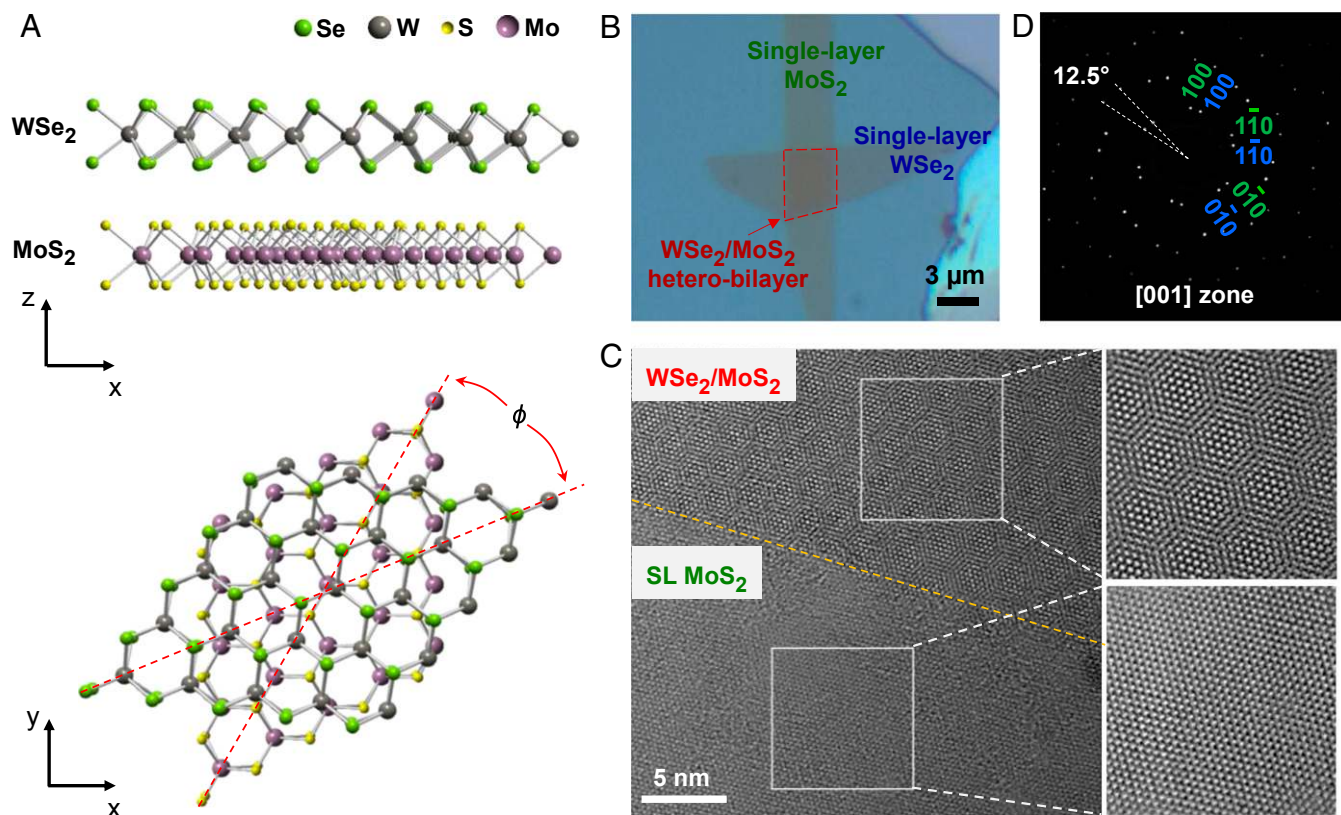


Fig. 1. WSe_2/MoS_2 hetero-bilayer illustration, optical image, and TEM images. (A) Atomistic illustrations of the heterostructure of single-layer (SL) WSe_2 on SL MoS_2 with their respective lattice constants and a misalignment angle ϕ . (B) Optical microscope image of a WSe_2/MoS_2 hetero-bilayer on a Si/SiO_2 substrate (260-nm SiO_2). (C) HRTEM images of a boundary region of SL MoS_2 and the hetero-bilayer, showing the resulting Moiré pattern. (D) The electron diffraction pattern of the hetero-bilayer shown in B, with the pattern of MoS_2 and WSe_2 indexed in green and blue colors, respectively.

single-layer MoS_2 and the WSe_2/MoS_2 hetero-bilayer. Whereas MoS_2 exhibits a simple hexagonal lattice, the heterostructure shows moiré fringes with a spatial envelope periodicity on the order of four to six times the lattice constants of WSe_2 (or MoS_2). Inspection of the diffraction pattern in Fig. 1D along the [001] zone axis reveals that in this particular sample the two hexagonal reciprocal lattices are rotated by $\phi=12.5^\circ$ with respect to each other and there is negligible strain in the two constituent layers (*Supporting Information*). The alignment of the two lattices can also be examined with a fast Fourier transform of the two zoomed-in TEM images in Fig. 1C (Fig. S1). The absence of strain in the constituent layers of the WSe_2/MoS_2 hetero-bilayer is also confirmed by Raman spectroscopy (Fig. S2), which show that the in-plane vibration modes of both WSe_2 and MoS_2 maintain their corresponding positions before and after transfer.

To shed light on the electronic structure of the WSe_2/MoS_2 heterostructure, we performed X-ray photoelectron spectroscopy (XPS). Specifically, we used a photoemission electron microscope (PEEM) with a high spatial resolution of 30 nm to discriminate between photoelectrons emitted from the WSe_2 single layer, MoS_2 single layer, and the WSe_2/MoS_2 hetero-bilayer, as illustrated in Fig. 2A (see Fig. S3 for details). In addition, by looking at the core-level photoelectrons, we achieved elemental and electronic selectivity that allows us to probe photoelectrons originating from the top layer of the hetero-bilayer and to directly quantify the potential difference between the WSe_2 layer in the hetero-stack with respect to the WSe_2 single-layer reference on the substrate. As shown in Fig. 2B, a peak shift of about -220 meV in binding energy (or $+220$ meV in kinetic energy) is evident in the W 4f core levels of the hetero-bilayer compared with the WSe_2 single layer. The direction of the peak shift is

consistent with a negative net charge on the WSe_2 in the WSe_2/MoS_2 hetero-bilayer. However, a shift of $+190$ meV is observed in the Mo 3d core levels of the WSe_2/MoS_2 in Fig. 2C. Our PEEM results therefore indicate that the WSe_2 layer has a negative net charge, whereas the MoS_2 layer has a positive net charge as a result of contact potential. The hetero-bilayer can essentially be interpreted as being a 2D dipole, an atomically thin parallel plate capacitor with vdW gap with a built-in potential up to 400 meV, originating from the work function difference induced charge transfer between the two constituent single layers. The latter interpretation is also consistent with the p- and n-type character of WSe_2 and MoS_2 , respectively (2, 3).

To investigate the optoelectronic properties of the WSe_2/MoS_2 hetero-bilayer, we used photoluminescence (PL) and absorption spectroscopy. It is known that both single-layer WSe_2 and MoS_2 exhibit direct band gaps, whereas their bulk and homo-bilayer counterparts are indirect (1, 27). In agreement with previous work we observe strong excitonic PL peaks at 1.64 eV and 1.87 eV for single-layer WSe_2 and MoS_2 , respectively (Fig. 3A). Note that single-layer WSe_2 shows a 10–20 times higher PL intensity than single-layer MoS_2 , a result consistent with ref. 28. For the WSe_2/MoS_2 hetero-bilayer, we observe a peak at 1.55 eV, lying interestingly at a lower energy than for the two constituent single layers, as shown in Fig. 3A (with intensity ~ 1.5 times higher than for single-layer MoS_2). The appearance of a peak at such low energy was observed consistently for multiple (>10) samples, with peak energies ranging from 1.50 to 1.56 eV (Fig. S4). This distribution is attributed to sample-to-sample variations in interface quality and/or alignment angle ϕ . Of value in optoelectronics, an Urbach tail inverse slope, corresponding to the band edge sharpness of ~ 30 meV/dec is extracted

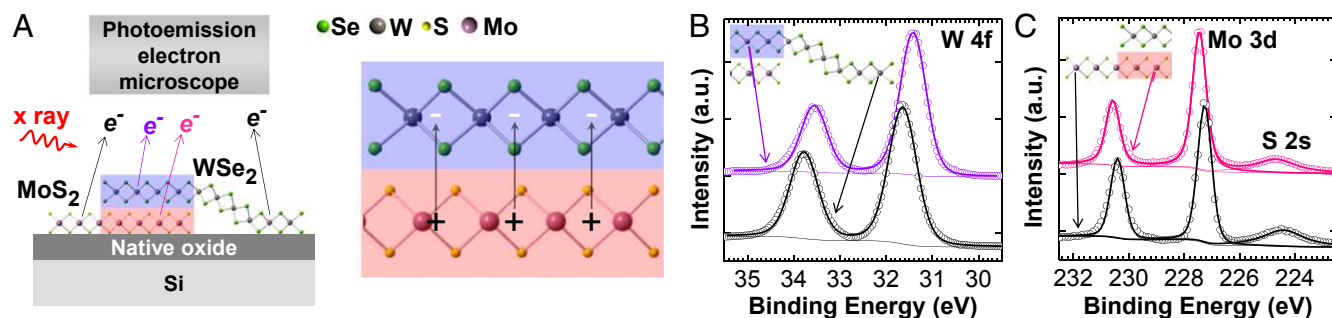


Fig. 2. XPS core level shift analyses of WSe_2/MoS_2 heterostructures. (A) Sketch of the spatially resolved PEEM experiment. (B) Comparison of W 4f core level doublet from WSe_2 and WSe_2/MoS_2 indicating a 220-meV shift to lower binding energy, corresponding to a negative net charge on the WSe_2 top layer. (C) Comparison of Mo 3d core level doublet and S 2s singlet from MoS_2 and WSe_2/MoS_2 indicating a shift of 190 meV to higher binding energy, corresponding to a positive net charge on MoS_2 . The single peak at 224.4–224.6 eV is identified as S 2s, which shows the same shift as Mo 3d, as expected.

from the PL spectra (29, 30) (Fig. S5). The steep tail slopes of our hetero-bilayer prove that high-quality heterostructures with sharp band edges can be built at the single-layer limit using TMDC building blocks, which is a unique feature of this material system.

The nature of the photoluminescence of the WSe_2/MoS_2 hetero-bilayer is intriguing. To better understand the electronic structure of the hetero-bilayer, we performed absorption measurements in the near-infrared and visible part of the spectrum using synchrotron light shown as dashed lines in Fig. 3B. The WSe_2/MoS_2 hetero-bilayer shows a first absorption peak at 1.65 eV and a second peak at 1.91 eV. These peaks closely coincide with the absorption peaks of single-layer WSe_2 and MoS_2 ,

respectively. Interestingly, comparing the absorption spectra with the normalized PL data shown in Fig. 3B, we note that the hetero-bilayer exhibits a striking ~ 100 meV shift between the PL and absorbance peaks. This large Stokes-like shift is consistent with a spatially indirect transition in a staggered gap (type II) heterostructure (31) (as shown in Fig. 3C). Our hetero-bilayers share certain similarities with organic semiconductor heterostructures in which donor and acceptor layers are also bound by weak intermolecular vdW forces (32). Similar to the optical processes in organic heterostructures, photons are absorbed in single-layer WSe_2 and single-layer MoS_2 , generating excitons in both layers. Photo-excited excitons then relax at the MoS_2/WSe_2

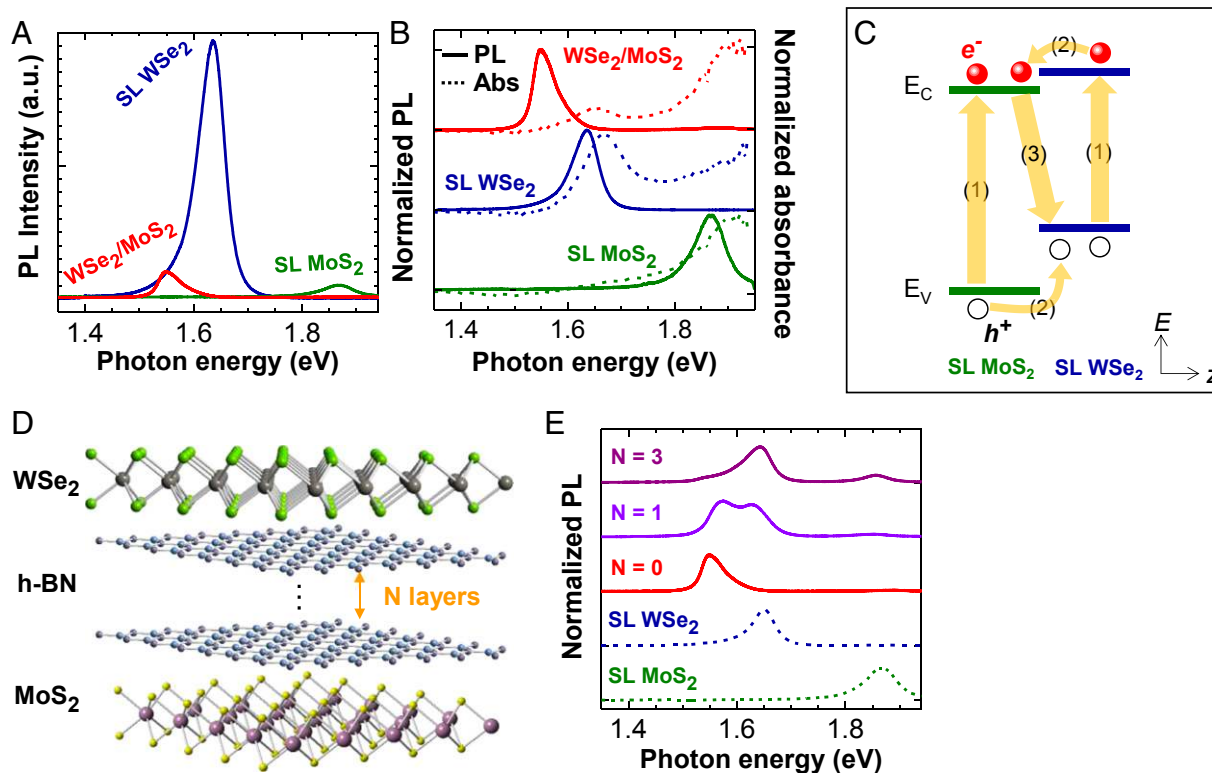


Fig. 3. Photoluminescence and absorption from WSe_2/MoS_2 hetero-bilayers. (A) PL spectra of single-layer WSe_2 , MoS_2 , and the corresponding hetero-bilayer. (B) Normalized PL (solid lines) and absorbance (dashed lines) spectra of single-layer WSe_2 , MoS_2 , and the corresponding hetero-bilayer, where the spectra are normalized to the height of the strongest PL/absorbance peak. (C) Band diagram of WSe_2/MoS_2 hetero-bilayer under photo excitation, depicting (1) absorption and exciton generation in WSe_2 and MoS_2 single layers, (2) relaxation of excitons at the MoS_2/WSe_2 interface driven by the band offset, and (3) radiative recombination of spatially indirect excitons. (D) An atomistic illustration of the heterostructure of single-layer WSe_2 /single-layer MoS_2 with few-layer h-BN spacer in the vdW gap. (E) Normalized PL spectra from single-layer WSe_2 /single-layer MoS_2 heterostructure with n layers of h-BN ($n = 0, 1, \text{ and } 3$).

1. Mak KF, Lee C, Hone J, Shan J, Heinz TF (2010) Atomically thin MoS₂: A new direct-gap semiconductor. *Phys Rev Lett* 105(13):136805.
2. Radisavljevic B, Radenovic A, Brivio J, Giacometti V, Kis A (2011) Single-layer MoS₂ transistors. *Nat Nanotechnol* 6(3):147–150.
3. Fang H, et al. (2012) High-performance single layered WSe₂ p-FETs with chemically doped contacts. *Nano Lett* 12(7):3788–3792.
4. Wang H, et al. (2012) Integrated circuits based on bilayer MoS₂ transistors. *Nano Lett* 12(9):4674–4680.
5. Zeng H, Dai J, Yao W, Xiao D, Cui X (2012) Valley polarization in MoS₂ monolayers by optical pumping. *Nat Nanotechnol* 7(8):490–493.
6. Jones AM, et al. (2013) Optical generation of excitonic valley coherence in monolayer WSe₂. *Nat Nanotechnol* 8(9):634–638.
7. Geim AK, Grigorieva IV (2013) Van der Waals heterostructures. *Nature* 499(7459):419–425.
8. Yu WJ, et al. (2013) Vertically stacked multi-heterostructures of layered materials for logic transistors and complementary inverters. *Nat Mater* 12(3):246–252.
9. Georgiou T, et al. (2013) Vertical field-effect transistor based on graphene-WSe₂ heterostructures for flexible and transparent electronics. *Nat Nanotechnol* 8(2):100–103.
10. Yu WJ, et al. (2013) Highly efficient gate-tunable photocurrent generation in vertical heterostructures of layered materials. *Nat Nanotechnol* 8(12):952–958.
11. Britnell L, et al. (2013) Strong light-matter interactions in heterostructures of atomically thin films. *Science* 340(6138):1311–1314.
12. Wilson J, Yoffe A (1969) The transition metal dichalcogenides discussion and interpretation of the observed optical, electrical and structural properties. *Adv Phys* 18(73):193–335.
13. Terrones H, López-Urías F, Terrones M (2013) Novel hetero-layered materials with tunable direct band gaps by sandwiching different metal disulfides and diselenides. *Sci Rep* 3:1549.
14. Kang J, Li J, Li S-S, Xia J-B, Wang L-W (2013) Electronic structural Moiré pattern effects on MoS₂/MoSe₂ 2D heterostructures. *Nano Lett* 13(11):5485–5490.
15. Košmider K, Fernández-Rossier J (2013) Electronic properties of the MoS₂-WSe₂ heterojunction. *Phys Rev B* 87(7):075451.
16. Komsa H-P, Krasheninnikov AV (2013) Electronic structures and optical properties of realistic transition metal dichalcogenide heterostructures from first principles. *Phys Rev B* 88(8):085318.
17. Gong C, et al. (2013) Band alignment of two-dimensional transition metal dichalcogenides: Application in tunnel field effect transistors. *Appl Phys Lett* 103(5):053513.
18. Dean CR, et al. (2010) Boron nitride substrates for high-quality graphene electronics. *Nat Nanotechnol* 5(10):722–726.
19. Ponomarenko L, et al. (2011) Tunable metal-insulator transition in double-layer graphene heterostructures. *Nat Phys* 7(12):958–961.
20. Haigh SJ, et al. (2012) Cross-sectional imaging of individual layers and buried interfaces of graphene-based heterostructures and superlattices. *Nat Mater* 11(9):764–767.
21. Britnell L, et al. (2012) Field-effect tunneling transistor based on vertical graphene heterostructures. *Science* 335(6071):947–950.
22. Gorbachev R, et al. (2012) Strong Coulomb drag and broken symmetry in double-layer graphene. *Nat Phys* 8:896–901.
23. Hunt B, et al. (2013) Massive Dirac fermions and Hofstadter butterfly in a van der Waals heterostructure. *Science* 340(6139):1427–1430.
24. Ponomarenko LA, et al. (2013) Cloning of Dirac fermions in graphene superlattices. *Nature* 497(7451):594–597.
25. Dean CR, et al. (2013) Hofstadter's butterfly and the fractal quantum Hall effect in moiré superlattices. *Nature* 497(7451):598–602.
26. Yankowitz M, et al. (2012) Emergence of superlattice Dirac points in graphene on hexagonal boron nitride. *Nat Phys* 8(5):382–386.
27. Zeng H, et al. (2013) Optical signature of symmetry variations and spin-valley coupling in atomically thin tungsten dichalcogenides. *Sci Rep* 3:1608.
28. Zhao W, et al. (2013) Evolution of electronic structure in atomically thin sheets of WS₂ and WSe₂. *ACS Nano* 7(1):791–797.
29. Van Roosbroeck W, Shockley W (1954) Photon-radiative recombination of electrons and holes in germanium. *Phys Rev* 94(6):1558.
30. Kost A, Lee H, Zou Y, Dapkus P, Garmire E (1989) Band-edge absorption coefficients from photoluminescence in semiconductor multiple quantum wells. *Appl Phys Lett* 54(14):1356–1358.
31. Wilson BA (1988) Carrier dynamics and recombination mechanisms in staggered-alignment heterostructures. *IEEE J Quantum Electron* 24(8):1763–1777.
32. Li G, Zhu R, Yang Y (2012) Polymer solar cells. *Nat Photonics* 6(3):153–161.
33. Jariwala D, et al. (2013) Gate-tunable carbon nanotube-MoS₂ heterojunction p-n diode. *Proc Natl Acad Sci USA* 110(45):18076–18080.
34. Chuang S, et al. (2013) Near-ideal electrical properties of InAs/WSe₂ van der Waals heterojunction diodes. *Appl Phys Lett* 102(24):242101.